Scripta Materialia 218 (2022) 114776

Contents lists available at ScienceDirect

Scripta Materialia

journal homepage: www.journals.elsevier.com/scripta-materialia

Domination of phononic scattering in solid solutioning and interfaces of HfB_2–ZrB_2 – SiC -carbon nanotube based ultra high temperature composites

Shruti Dubey [a], Ariharan S [a,b], Ambreen Nisar [a,c], Sudha Saini [a], Subhra S. Jana [a], Bhimashankar Wangaskar [d], Amit Das [a,e], Sameer Khandekar [d], Tanmoy Maiti [a], Shobit Omar [a], Kantesh Balani [a,f,*]

[a] Department of Materials Science and Engineering, Indian Institute of Technology Kanpur, Kanpur, 208016, Uttar Pradesh, India
[b] Currently at Department of Coating Processes, Alexander Dubcek University of Trencin, Slovakia
[c] Currently at Department of Mechanical and Materials Engineering, 10555 West Flagler Street, Miami, FL 33174, United States
[d] Department of Mechanical and Materials Engineering, Indian Institute of Technology Kanpur, Kanpur, 208016, Uttar Pradesh, India
[e] Centre for Ceramics Processing, International Advanced Research Centre for Powder Metallurgy and New Materials, Hyderabad, Telangana, 500005, India
[f] Advanced Centre for Materials Science, Indian Institute of Technology Kanpur, Kanpur, 208016, Uttar Pradesh, India

ARTICLE INFO

Keywords:
Ultra high temperature ceramics (ZrB_2, HfB_2)
Thermal conductivity
Phonon scattering
Solid solution

ABSTRACT

HfB_2-ZrB_2 based ultra-high temperature ceramics (UHTCs) are used as protective tiles for nose cones and leading edges of the hypersonic vehicles that face harsh service conditions of temperatures >2000 °C. The present work assesses the effect of SiC (20 vol.%) and carbon nanotubes (CNT, 6 vol.%) incorporation on isolating the phononic and electronic contribution to thermal conductivity of spark plasma sintered HfB_2-ZrB_2 based UHTCs. Except HfB_2-SiC, all ZrB_2 based UHTC composites elicited similar electrical conductivity (~ 5.7×10^6 S/m), whereas a marginal increase of ~9% in thermal conductivity was observed with CNT reinforcement in HfB_2-ZrB_2–SiC composites. With HfB_2/ZrB_2-SiC composites eliciting high thermal conductivity (120–150 $Wm^{-1}K^{-1}$), the current work emphasizes the domination of phononic scattering (by ~44%) due to solid solutioning in HfB_2-ZrB_2-based ceramics. Further, electronic thermal scattering events may only be marginal at interfaces of CNT and ZrB_2, and limit thermal scattering in HfB_2/ZrB_2-SiC-CNT based UHTCs for hypersonic applications.

High thermal conductivity (κ) is mandated in sharp-leading edge applications in order to avoid formation of hot spots and lower the thermal stresses [1–3]. High thermal conductivity (κ) of ZrB_2/HfB_2 based materials falls within the threshold application needs (~60–80 $Wm^{-1}K^{-1}$). The thermal conduction is a function of both phononic and electronic contributions. Typically, monolith borides have shown dominance of electronic contribution (~65%) with only assisted thermal scattering from phononic events (~35%). But, the effect of solid-solutioning and incorporating the CNT, SiC, reinforcements in HfB_2/ZrB_2 systems need attention so as to curb thermal scattering events and enhance the overall thermal conductivity.

SiC is an established reinforcement incorporated in the HfB_2/ZrB_2 matrix making it mechanically and thermally sustainable under extreme environment conditions [4–7]. An anomalous thermal conductivity of ZrB_2 based on processing (hot pressing and SPS) and reinforcements (SiC, $MoSi_2$, C) is well reported in literature [7]. On one hand, SiC (~125 $Wm^{-1}K^{-1}$) [8] incorporation in ZrB_2 matrix led to lower thermal conductivity values (~87.0 $Wm^{-1}K^{-1}$ [9]) than that of the monolith (~108 $Wm^{-1}K^{-1}$ [9]) at 298 K or 25 °C (highlighting the interfacial thermal scattering effect). Whereas, in another work, synergistic reinforcement of SiC and CNT have exhibitied a higher thermal conductivity of 61.8 $Wm^{-1}K^{-1}$ at 50 °C, or 323 K, and of 52.3 $Wm^{-1}K^{-1}$ at 1200 °C, or 1473 K when compared to that of monolith ZrB_2 (~48.9 $Wm^{-1}K^{-1}$ at 50 °C, and 42.3 $Wm^{-1}K^{-1}$ at 1200°C) [10] . A crossover of higher thermal conductivity of SiC reinforced ZrB_2 (89.5 $Wm^{-1}K^{-1}$ decreased to ~74.8 $Wm^{-1}K^{-1}$ at 1000 °C or 1273 K) is also reported in literature with respect to that of monolithic ZrB_2 (i.e. 83.8 $Wm^{-1}K^{-1}$ at 25 °C, and 81.8 $Wm^{-1}K^{-1}$ at 1000 °C) [7]. Concurrently, SiC addition alone exhibited similar thermal conductivity ~50-52 $Wm^{-1}K^{-1}$ at 1200 °C, when compared to that with synergistic SiC and CNT reinforcement in ZrB_2 [10]. The κ of 20 vol% SiC reinforced HfB_2 (~141 $Wm^{-1}K^{-1}$) or ZrB_2 (~89.5 $Wm^{-1}K^{-1}$) composites consolidated via hot pressing at 2000 °C for 30 min (uniaxial pressure~30 MPa) have reported an increase in room temperature κ > 30% for HfB_2-SiC composites and 7% for ZrB_2-SiC [7]. κ_{SiC} is a function

* Corresponding author.
E-mail address: kbalani@iitk.ac.in (K. Balani).

https://doi.org/10.1016/j.scriptamat.2022.114776
Received 21 March 2022; Accepted 27 April 2022
Available online 14 May 2022

of phonon transport which reduces drastically in presence of impurities such as WC introduced during milling, thus, lowering the κ of the diboride based ceramic [11]. The room temperature κ of ZrB_2 also decreases by ~40% on introduction of HfB_2 in the matrix without much difference in charge carrier density (similar electronic structure, AlB_2) but rather, due to difference in phonon scattering and formation of solid solution of (Hf-Zr)B_2 [12]. CNT, on the other hand, not only improves densification but works synergistically to enhance the thermal and electrical transport in diboride based composites [10,13,14]. The addition of 10 vol% CNT to ZrB_2 + 20 vol% SiC has elicited marginal increase in high temperature (1200 °C) thermal conductivity to ~52.3 $Wm^{-1}K^{-1}$ [10].

The spark plasma sintering (SPS) of (Hf,Zr)B_2-SiC-CNT system (at 1850 °C, 30 MPa for 10 min hold time, vacuum ~6 Pa) is reported earlier highlighting the solid solution, and eliciting enhanced mechanical (H~28.1 GPa, K_{IC}~10.2 $MPa.m^{1/2}$) [15] and tribological performance [16] with synergistic superior mechanical properties in HZ20S6C (37 vol.% HfB_2, 37 vol.% ZrB_2, 20 vol.% SiC and 6 vol.% CNT) compared to that of HZ20S.

Fig. 1i(a-i) [15] present the microstructural morphology of ZrB_2-HfB_2-based composites, and elemental spectrum of starting phase pure SiC, HfB_2 and ZrB_2 powders. Further, marginal increase in oxidation resistance (~6%) is depicted by HZ20S6C due to the synergistic solid solution, presence of CNT and SiO_2 formation on oxidation of SiC phase [17,18].

The current work focuses on isolating the effect of porosity, solid solutioning and reinforcements on the phononic and electronic contributions of thermal conductivity in HfB_2-ZrB_2 based UHTCs. The electrical conductivity of HfB_2-ZrB_2 based UHTCs makes these pliant to be machined by electrical discharge machining for near net shaping. To the best of our knowledge, it is for the first time that these phase-contribution aspects have been theoretically studied to explain the mechanism of thermal conduction as a function of electronic and phononic scattering.

The thermal diffusivity (D) measured using Netzsch LFA 447 Nanoflash™ with InSb infrared detector [19] using ($D = k\,L^2 t_{1/2}^{-1}$, Fig. 1 (ii)) where k is taken as 0.1388 and $t_{1/2}$ is presented in Table 1. Therein, a short laser pulse from xenon lamp (λ=150 nm-2000 nm) was flashed on the graphite coated sample (of 12.7 mm diameter and ~2–2.5 mm thickness (L)) with emissivity of ~1. From which laser flash longitudinal thermal conductivity ($\kappa = D\rho C_p$) of HfB_2-ZrB_2-based composites is calculated (*Fig. 1*(iii), and see Appendix eq. A1 and A2) where C_p~0.779 $Jg^{-1}K^{-1}$ and ρ is the density of the sample. It was observed that the κ_{H20S} (~124 $Wm^{-1}K^{-1}$) and κ_{Z20S} (~153 $Wm^{-1}K^{-1}$) are both ~ 16% more than

Table 1
Nomenclature based on composition of consolidated samples, density(ρ), porosity, half-time ($t_{1/2}$) for estimation of thermal conductivity.

Sample ID	Composition (Vol%) HfB_2	ZrB_2	SiC	CNT	ρ [15] (gcm^{-3})	Porosity [15](%)	$t_{1/2}$ (s)
H20S	80	0	20	0	9.04	0.00	0.032 ±0.001
Z20S	0	80	20	0	5.46	1.00	0.022 ±0.000
HZ20Sf	40	40	20	0	6.98	4.00	0.047 ±0.000
HZ20S6C	37	37	20	6	6.85	0.05	0.036 ±0.001

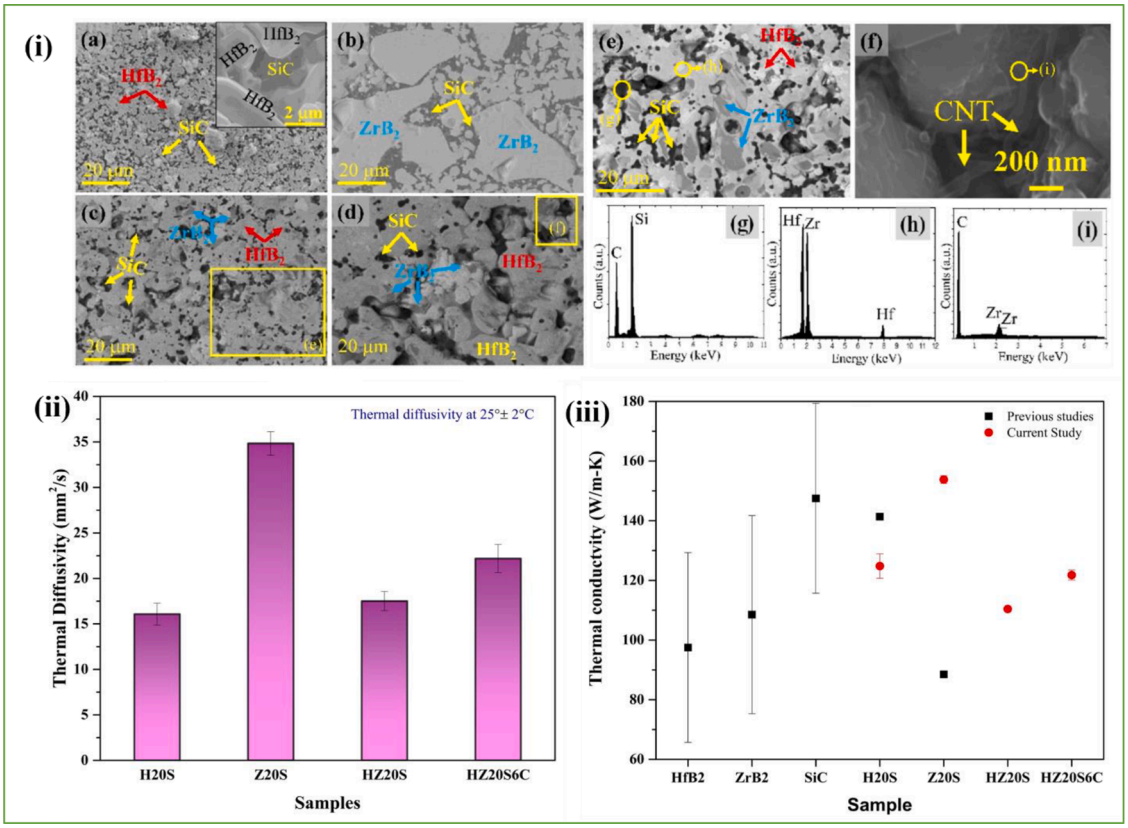

Fig. 1. (i) SEM micrograph of (a) H20S, (b) Z20S (c) HZ20S (d) HZ20S6C (e) Solid solution of (Hf-Zr)B_2 in HZ20S (f) presence of CNTs in HZ20S6C and energy dispersive spectroscopy of (g) SiC, (h) HfB_2 and (i) ZrB_2 (images a-i: Open access, Coatings (MDPI, [15]), (ii) Experimentally measured average thermal diffusivity, and (iii) corresponding comparison of previously reported and experimentally obtained thermal conductivity of HfB_2, ZrB_2, SiC and HfB_2-ZrB_2-based UHTCs. The room temperature thermal conductivity of HfB_2, ZrB_2, SiC and CNT is taken as 75–120 $Wm^{-1}K^{-1}$ [36], 85–132 $Wm^{-1}K^{-1}$ [8,20], 125–170 $Wm^{-1}K^{-1}$ [8], and 1000–2000 $Wm^{-1}K^{-1}$ [27], respectively. κH20S and κZ20S are reported ~141 $Wm^{-1}K^{-1}$ and ~89.53 $Wm^{-1}K^{-1}$, respectively [7].

their corresponding phase pure HfB_2 (~107 $Wm^{-1}K^{-1}$ [20]) and ZrB_2 (~132 $Wm^{-1}K^{-1}$ [20]) . Also, κ_{H20S} is 18% less than κ_{Z20S} despite being 100% dense, which may be attributed to poor sintering of H20S (as sintering was optimized with respect to that of ZrB_2-systems [21]). The least κ value observed in HZ20S (~110 $Wm^{-1}K^{-1}$) is attributed to the presence of pores (~4%, κ_{pore} ~0.4 $Wm^{-1}K^{-1}$) in the HfB_2-ZrB_2 matrix resulting in an overall reduction of ~28% and 11% when compared to that of Z20S, and H20S, respectively. Incorporation of highly conducting CNTs (~6 vol%) raised the κ_{HZ20S} by ~9% in HZ20S6C (~121 $Wm^{-1}K^{-1}$) as a combined effect of reduction of porosity (~0.5%) along with incorporation of high κ_{CNT} (~ 1000–2000 $Wm^{-1}K^{-1}$). However, a marginal decrease in $\kappa_{HZ20S6C}$ as compared to that of H20S (~2% decrease) and Z20S (~26% decrease), which is attributed to random distribution of CNT (refer [21], whereas its alignment has elicited higher κ in literature [22,23]).

Effect of microstructure (i.e., as grain boundaries, porosity, carbon nanotube content and orientation, interphase boundary, and phase content) on thermal conductivity is presented in Appendix Table A1. A low κ_{mn} (~ 71.3 $Wm^{-1}K^{-1}$) of H20S indicates the dominance of interfacial scattering (grain size of ~7–10 μm [21]) when compared to that of Z20S (~99 $Wm^{-1}K^{-1}$ with grain size of ~10–20 μm [21]). Assuming no solid solution formation, a lower theoretical thermal-conductivity estimate (~91 $Wm^{-1}K^{-1}$) indicates interfacial scattering in HZ20S, whereas an overestimate of thermal conductivity of HZ20S6C (~176 $Wm^{-1}K^{-1}$) may be attributed to using inherently high thermal conductivity value of CNT (~2000 $Wm^{-1}K^{-1}$). These estimations does not lie in range with experimental observations, which may be attributed to porosity and (Hf, Zr)B_2 solid-solution formation. Further, the contribution of individual phases (HfB_2, ZrB_2, SiC and CNT) to κ for 100% dense HfB_2 - ZrB_2 based composites on thermal conductivity was estimated via Rule of Mixture (ROM, without accounting for pores/interfaces, Fig. 2(i)). The theoretical thermal conductivity estimation of H20S by ROM is ~7.4% higher than its experimental value, affirming interfacial resistance.

It may be noted that Fig. 1(i) indicates higher porosity content in HfB_2 containing samples than that of its reported Archimedes density value (~100% dense [21]) as the process variables were optimized with respect to that of ZrB_2. On the other hand, ~23% and 54% difference in the theoretical estimates and experimental thermal conductivity of HZ20S and HZ20S6C, respectively, is accounted by the presence of porosity (in HZ20S, Fig. 2(ii)) and solid solution formation (HZ20S and HZ20S6C) Fig. 2(i). As H20S, Z20S are fully dense compositions (Table 1) and, hence, thermal conductivity estimations are nearly similar to that of ROM, Fig. 2(i), however, lower κ value is observed for HZ20S, which is ~4% porous. For HZ20S, the Landauer [24], Meredith & Tobias [25] and Shafiro & Kachanov [26] models have shown κ values to vary from ~93.6 $Wm^{-1}K^{-1}$ to ~90.5 $Wm^{-1}K^{-1}$ and ~86.9 $Wm^{-1}K^{-1}$, respectively (refer to appendix Table A1). Close fitting of the Landauer's model with the experimental value (~110 $Wm^{-1}K^{-1}$) affirm porosity as major thermal scattering sites in HZ20S (Fig. 2(ii)). Out of 23.2% thermal conductivity decrease in HZ20S system, the contribution of porosity is ~6% (i.e., difference from ROM (κ_{mn}~ 144.2 $Wm^{-1}K^{-1}$) and Landauer model (κ_{mnp}~ 135.5 $Wm^{-1}K^{-1}$)), as shown in Fig. 2(ii). Thus, on comparing Fig. 2(i) and (ii), the remaining ~17.2% decrease in experimental thermal conductivity of HZ20S, then, may be attributed to solid solutioning.

Models based on effective medium approach (EMA) [27–29] are used to estimate the κ of CNT reinforced samples (κ_e, Fig. 2(ii)). It has been reported earlier that merely ~10 vol% CNTs can enhance the κ by up to 70% [30]. The estimation by Xue model [29] considering poor dispersion of CNTs (~220 $Wm^{-1}K^{-1}$) is still ~81% more than the experimental thermal conductivity value of HZ20S6C (~121 $Wm^{-1}K^{-1}$, also refer to Table A1 in appendix). First, it may be noted that though Archimedes

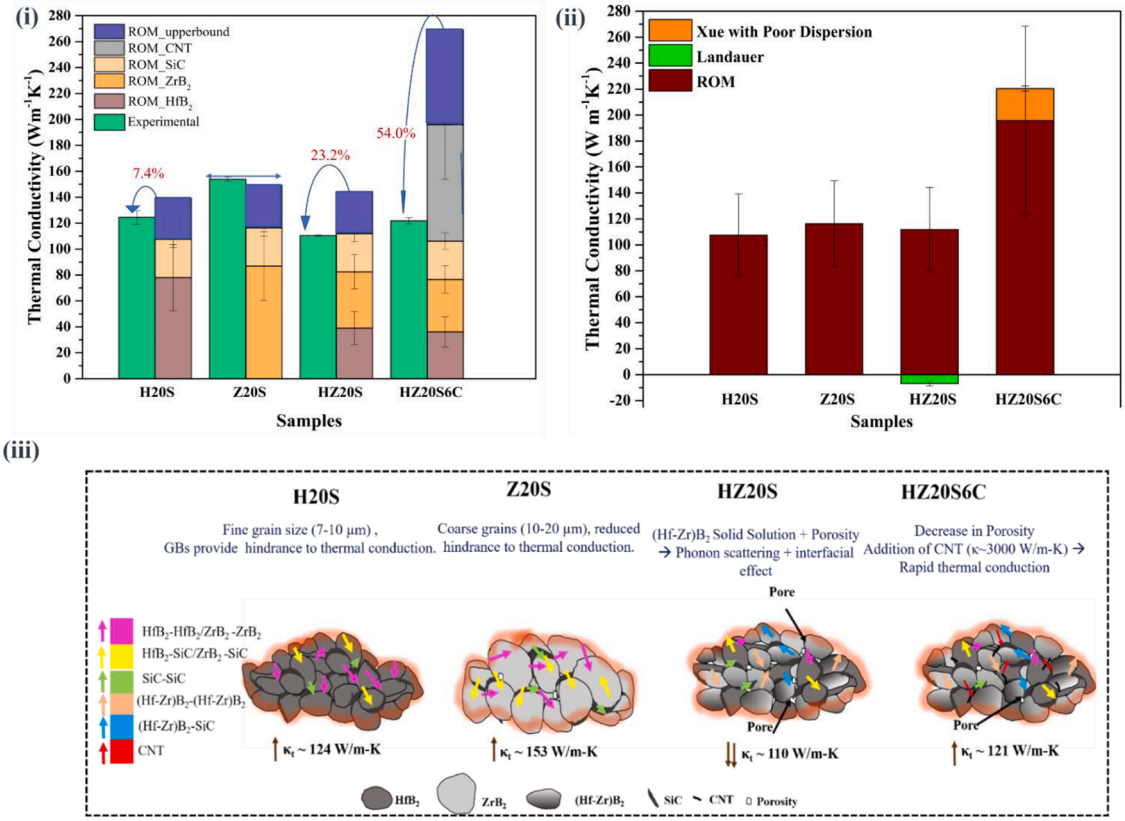

Fig. 2. (i) Theoretical quantification and isolated contribution of each phase on thermal conductivity with respect to that of experimental values (maximum value from Rule of Mixture is taken to provide the effect), and (ii) contribution of pores and CNTs with respect to ROM. (iii) Schematic representation of effect of grain boundary, phases, porosity and CNT on thermal conductivity of H20S, Z20S, HZ20S and HZ20S6C.

density of HZ20S is reported to be nearly fully dense [21], the microstructure does elicit porosity (which might be attributed to solid solution formation). Thus, ~17% contribution of decrease in thermal conductivity (in HZ20S sample) is supplemented with ~37% thermal scattering at interface (due to porosity and interfaces of CNTs and otherwise) to result a net 54% decrease from the maximum theoretical estimates (Fig. 2(ii)) in HZ20S6C. Secondly, enhanced scattering due to interfaces/porosity, and phonic scattering in solid solutioning phase, the addition of CNTs has still contributed a minor increase in the overall thermal conductivity.

An overall enhancement in $\kappa_{HZ20S6C}$ is ~10% with respect to κ_{HZ20S} achieving full densification and increased thermal conduction due to CNTs distributed in HZ20S matrix. In case of HZ20S (~110 $Wm^{-1}K^{-1}$), porosity acts as a thermal dissipation site, which is overcome by densification brought by nanofiller addition (of CNT) in HZ20S6C. It should be noted that none of the theoretical models discussed here consider the effect of solid solution formation.

Fig. 2(iii) schematically summarizes the dominance of microstructural features such as grain boundary, interfaces, pores and CNT in HfB_2-ZrB_2 matrix. H20S has fine grain structure (7–10 μm) when compared to that of Z20S (10–20 μm) and hence, the grain boundaries increase, which increases the thermal resistance due to thermal scattering by grain boundaries and interfaces (HfB_2 and SiC). H20S and Z20S are fully dense composites and negate any strong contribution of porosity, thus, the solid solution of HfB_2-ZrB_2 in HZ20S lead to the introduction of porosity (~4%) which have extremely low κ (~0.4 $Wm^{-1}K^{-1}$) and hence, play a dominant role in lowering κ_{HZ20S} (~110 $Wm^{-1}K^{-1}$). Further, (Hf-Zr)B_2 solid solution phase resist thermal conduction as an additional scattering interface with HfB_2, ZrB_2 and SiC. Therefore, solid solution formation in HZ20S is detrimental and reduces thermal conduction [1]. Whereas addition of CNT in HZ20S matrix (i.e. HZ20S6C) acts a nanofiller, enhancing densification (~ 99.5%), which, in turn, improves thermal conduction by more than 9% when compared to that of HZ20S.

As the total thermal conduction in diborides comprises both electronic and phononic component, electrical conductivity (σ_e) at room temperature has also been assessed. The electrical conductivity and Seebeck coefficient (S) of the HfB_2-ZrB_2-based composites was measured in the He atmosphere at room temperature using ZEM-3M10 apparatus (ULVAC-RICO Inc.). The figure of merit ($ZT = \frac{S^2\sigma_e T}{\kappa}$) was calculated, Table 2, from thermoelectric parameters (electrical conductivity and Seebeck coefficient). Seebeck coefficient is observed to be negative, suggesting n-type semiconductor behavior, with electrons to be dominant charge carriers in all the composites, and following similar trend of electrical conductivity at room temperature with maximum of -3.57 V/K observed for HZ20S6C. The power factor is ~6×10^{-5} $Wm^{-1}K^{-2}$ at room temperature for Z20S, HZ20S and HZ20S6C composites (Table 2) except for H20S (where the presence of HfB_2 phase dominates). On the other hand, ZT value for Z20S is ~43 times to that of H20S. After incorporation of CNT, all thermoelectric parameters in HZ20S6C are observed to increase ~4–6% as compared to that of HZ20S. Low ZT value in ~1×10^{-4} $Wm^{-1}K^{-1}$ range (due to high κ) for these composites is not sufficient for thermoelectric applications at room temperature.

The experimental electrical conductivity at room temperature is maximum for Z20S (~5.69×10^6 Sm^{-1}), which is ~ 2.85 times (~1.99×10^6 Sm^{-1}) to that of H20S owing to inherently high electrical conductivity of pure ZrB_2 (~1.0×10^7 Sm^{-1} [8,9]) than HfB_2 (~9.1×10^6 Sm^{-1} [9]). However, SiC is the least electrically conducting phase (~10^2 Sm^{-1} [9]) in all the four compositions, thus, acting as electronic scattering centers. The σ_e is comparable (~$5.6–5.7 \times 10^6$ Sm^{-1}) for Z20S, HZ20S and HZ20S6C (~0.01×10^6 Sm^{-1}). To obtain complex electron interaction in HZ20S and HZ20S6C, the effects of porosity and grain size are normalized where on the other hand the formation of solid solution is taken into consideration which restricts the electron motion due to the hindrance by intermixed electrons of Hf/ZrB_2 [31] . Thus, a slight increase in electrical conductivity (~5%) of HZ20S is a combined effect of solid solution formation and presence of porosity (<4%). The electrical conductivity further increases ~4% (~5.72×10^6 Sm^{-1}) on addition of CNT (σ_e~10^4 Sm^{-1}) to HZ20S.

Various studies have reported phonon conduction (κ_p) to be a significant (~35%) heat transport mechanism along with electronic conduction ($\kappa_{e,}$) contributions to total thermal conductivity, $(\kappa_t = \kappa_e + \kappa_p)$ in transition metal diborides [27]. Thus, extracting the contribution of phonon scattering on thermo-electrical transport in these composites may potentially help in designing lower κ thermoelectric materials. Table 2 enumerates κ_e and corresponding κ_p obtained for HfB_2-ZrB_2 based composites at room temperature (~303 K). It highlights that κ_p is high ~<60% of κ_t attributed to the presence of electrically insulating phase, i.e. SiC (σ>1000 μΩ-cm [32,33]) along with porosity (~4%) and the solid solution formation of (Hf-Zr)B_2 in HZ20S acting as phonon scattering centers and thereby restricting the electronic conduction (κ_e~44.9 $Wm^{-1}K^{-1}$) [2], which commensurate with study conducted by Tye and Clougherty [34]. It may be noted, Table 2, that high phonic contribution in both H20S and Z20S sample (~110 $Wm^{-1}K^{-1}$) has dropped to ~62–77 $Wm^{-1}K^{-1}$ in HZ20S and HZ20S6C samples (i.e. after formation of (Hf, Zr)B_2 solid solution). Pores (κ_{air}~0.4 $Wm^{-1}K^{-1}$) scatter phonons and also disrupt the electronic conduction. The phenomenon of solid solutioning is complex involving phonon scattering, while retaining the continual electron cloud conduction (probably through ZrB_2 channels in all ZrB_2 containing samples, Table 2) in HfB_2-ZrB_2-based composites when compared to that of H20S or Z20S [35]. On the other hand, addition of CNTs in the HZ20S matrix increases the overall phononic contribution (i.e. from 62 $Wm^{-1}K^{-1}$ to 76.9 $Wm^{-1}K^{-1}$, Table 2) to thermal conduction of HZ20S6C with negligible electronic contribution enhancement compared to that of HZ20S.

The mechanism of thermal conduction is summarized in schematic presentation shown in Fig. 3, highlighting the effect of porosity, solid solution and synergistic role of SiC and CNT on the phononic and electronic scattering in HfB_2- ZrB_2 based composites. The phononic conduction appears to primarily dominate heat conduction in HfB_2/ZrB_2.

Table 2
Thermoelectric parameters (Seebeck coefficient and Power factor), figure of merit and the phononic and electronic contribution to total thermal conductivity ($\boldsymbol{\kappa_p}$ and $\boldsymbol{\kappa_e}$) for HfB_2 – ZrB_2 based UHTCs at temperature of 310±2 K.

Sample ID	$\sigma_e \times 10^6$ (Sm^{-1})	$S \times 10^{-6}$ (VK^{-1})	P.F. $\times 10^{-5}$ ($Wm^{-1}K^{-2}$)	ZT $\times 10^{-4}$	κ_p ($Wm^{-1}K^{-1}$)	κ_e ($Wm^{-1}K^{-1}$)
H20S	1.99±0.11	−0.25±0.15	0.01±0.00	0.004±0.000	113.6±5.6	14.9±0.8
Z20S	5.69±0.04	−3.72±0.30	7.89±1.23	1.75±0.024	110.9±1.1	42.6±0.3
HZ20S	5.97±0.55	−3.34±0.72	6.68±2.20	1.79±0.746	62.3±3.4	44.9±4.2
HZ20S6C	5.72±0.41	−3.57±0.94	7.42±3.32	1.86±0.793	76.9±3.7	42.9±3.1

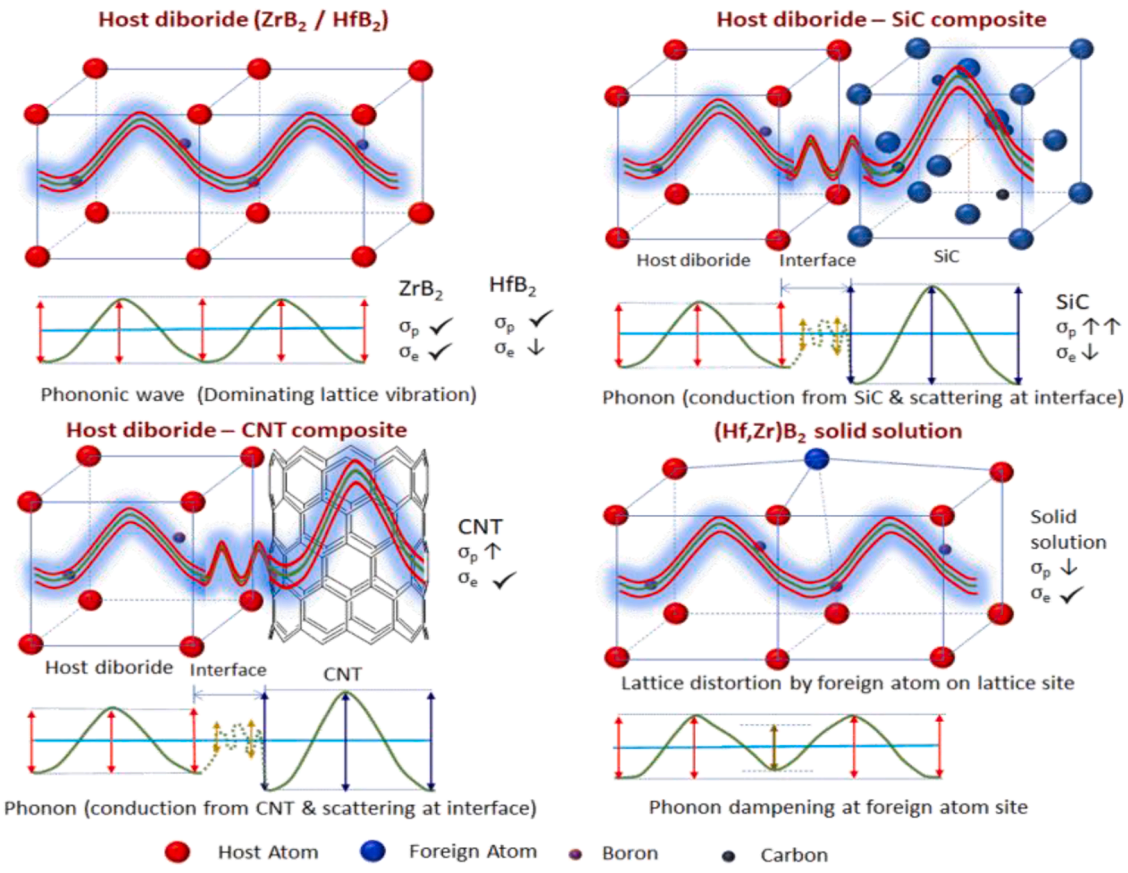

Fig. 3. Mechanism of thermal conduction highlighting the dominance of electronic and phononic contribution to thermal conduction in SiC and CNT reinforced HfB_2-ZrB_2 based UHTC.

SiC, reported to be situated at the grain boundary [23], increases the phonic contribution, and thus, thermal conductivity of H20S (from 75-120 $Wm^{-1}K^{-1}$ to 124.8 $Wm^{-1}K^{-1}$) and Z20S (from 85-132 $Wm^{-1}K^{-1}$ to 153.8 $Wm^{-1}K^{-1}$), Fig. 2(i). Thermal scattering occurs at HfB_2/ZrB_2-SiC and HfB_2/ZrB_2-CNT interfaces due to Kapitza resistance (Fig. 3) despite high thermal conductivity of SiC (125–170 $Wm^{-1}K^{-1}$) and CNT (2000–3000 $Wm^{-1}K^{-1}$) reinforcements. X-ray diffraction peak broadening in HZ20S and HZ20S6C [21] indicates lattice distortion due to the formation of (Hf-Zr)B_2 solid solution, results preferential phononic scattering, whereas electronic contribution is observed to sustain (Table 2) possibly due to its complex electron cloud.

Declaration of Competing Interest

The authors declare that they have no known competing financial interests or personal relationships that could have appeared to influence the work reported in this paper.

Acknowledgements

Dr. Rita Maurya is acknowledged for her technical assistance throughout this work. Dr. Niraj Mohan Chawake is also acknowledged for his technical insights and inputs. Mr. Indrajeet Singh is acknowledged for helping with the schematic. KB acknowledges funding from Indian Space Research Organization (Space Technology Cell at IIT Kanpur), and Impacting Research Innovation and Technology (IMPRINT, sanction number: IMP/2018/000739) from Science & Engineering Research Board (SERB), Department of Science & Technology, Govt. of India.

Supplementary materials

Supplementary material associated with this article can be found, in the online version, at doi:10.1016/j.scriptamat.2022.114776.

References

[1] W.G. Fahrenholtz, G.E. Hilmas, Scr. Mater. 129 (2017) 94–99.
[2] H. Bin Ma, J. Zou, J.T. Zhu, P. Lu, F.F. Xu, G.J. Zhang, Acta Mater 129 (2017) 159–169.
[3] H.K.M. Al-Jothery, T.M.B. Albarody, P.S.M. Yusoff, M.A. Abdullah, A. R. HusseinIOP Conf, Ser. Mater. Sci. Eng. 863 (2020).
[4] L. Silvestroni, H.J. Kleebe, W.G. Fahrenholtz, J. Watts, Sci. Rep. 7 (2017).
[5] S. Ghadami, E. Taheri-Nassaj, H.R. Baharvandi, F. Ghadami, Sci. Rep. 11 (2021) 1–11.
[6] S. Chakraborty, D. Debnath, A.R. Mallick, P.K... Das, Metall. Mater. Trans. A Phys. Metall. Mater. Sci. 45A (2014) 6277–6284.
[7] M. Mallik, A.J. Kailath, K.K. Ray, R. Mitra, J. Eur. Ceram. Soc. 32 (2012) 2545–2555.
[8] J.W. Zimmermann, G.E. Hilmas, W.G. Fahrenholtz, R.B. Dinwiddie, W.D. Porter, H. Wang, J. Am. Ceram. Soc. 91 (2008) 1405–1411.
[9] L. Zhang, D.A. Pejaković, J. Marschall, M. Gasch, J. Am. Ceram. Soc. 94 (2011) 2562–2570.
[10] A. Nisar, S. Ariharan, T. Venkateswaran, N. Sreenivas, K. Balani, Carbon 111 (2017) 269–282.
[11] W.G. Fahrenholtz, E.J. Wuchina, W.E. Lee, Y. Zhou, Ultra-High Temp. Ceram. Mater. Extrem. Appl. (2012) 1–5.
[12] A.D. Stanfield, G.E. Hilmas, W.G. Fahrenholtz, J. Eur. Ceram. Soc. 40 (2020) 3824–3828.
[13] A. Nisar, S. Ariharan, K. Balani, Direction 15 (2015) 55–65.
[14] A. Nisar, S. Ariharan, K. Balani, J. Mater. Res. 31 (2016) 682–692.
[15] A. Nisar, K. Balani, Coatings 07 (2017) 110.
[16] S. Dubey, S. Awasthi, A. Nisar, K. Balani, JOM 72 (2020) 2207–2218.
[17] R. Hassan, S. Omar, K. Balani, Int. J. Refract. Met. Hard Mater. 84 (2019), 105041.
[18] R. Hassan, K. Balani, Corros. Sci. 177 (2020).
[19] NETZSCH Pumps and Systems, 2022 LFA 447 NanoFlash (n.d.).
[20] W.G. Fahrenholtz, E.J. Wuchina, W.E. Lee, Y. Zhou, Ultra-High Temperature Ceramics: Materials for Extreme Environment Applications, John Wiley & Sons, Inc, Hoboken, NJ, 2014.

[21] A. Nisar, K. Balani, Coatings 7 (2017).
[22] T.A. Parthasarathy, R.A. Rapp, M.M. Opeka, R.J. Kerans, Acta Mater 55 (2007) 5999–6010.
[23] S. Ariharan, B. Wangaskar, V. Xavier, T. Venkateswaran, K. Balani, Ceram. Int. 45 (2019) 18951–18964.
[24] R. Landauer, J. Appl. Phys. 23 (1952) 779–784.
[25] F. Cernuschi, S. Ahmaniemi, P. Vuoristo, T. Mäntylä, J. Eur. Ceram. Soc. 24 (2004) 2657–2667.
[26] B. Shafiro, M. Kachanov, J. Appl. Phys. 87 (2000) 8561–8569.
[27] C.W. Nan, Z. Shi, Y. Lin, Chem. Phys. Lett. 375 (2003) 666–669.
[28] C.W. Nan, G. Liu, Y. Lin, M. Li, Appl. Phys. Lett. 85 (2004) 3549–3551.
[29] Q.Z. Xue, Condens. Matter 368 (2005) 302–307.
[30] R. Sivakumar, S. Guo, T. Nishimura, Y. Kagawa, Scr. Mater. 56 (2007) 265–268.
[31] G. Harrington, Effect of solid solutions and second phases on the thermal conductivity of zirconium diboride ceramics, 2014.
[32] W.G. Fahrenholtz, G.E. Hilmas, I.G. Talmy, J.A. Zaykoski, J. Am. Ceram. Soc. 90 (2007) 1347–1364.
[33] X. Zhang, G.E. Hilmas, W.G. Fahrenholtz, J. Am. Ceram. Soc. 91 (2008) 4129–4132.
[34] W.G. Fahrenholtz, E.J. Wuchina, W.E. Lee, Y. Zhou, in: Wiley, 2014.
[35] M. Murabayashi, J. Nucl. Sci. Technol. 7 (1970) 559–563.
[36] G.V. Samsonov, T.I. Serebryakova, Sov. Powder Metall. Met. Ceram. 17 (1978) 116–120.